

IXPE Detection of Polarized X-rays from Magnetar and Photon Mode Conversion at QED Vacuum Resonance

Dong Lai*

Cornell Center for Astrophysics and Planetary Science, Department of Astronomy, Cornell University, Ithaca, NY 14853

September 29, 2022

The recent observation of the anomalous X-ray pulsar 4U 0142+61 by the Imaging X-ray Polarimetry Explorer (IXPE) opened up a new avenue to study magnetars, neutron stars endowed with superstrong magnetic fields ($B \gtrsim 10^{14}$ G). The detected polarized X-rays exhibit an intriguing 90° linear polarization swing from low photon energies ($E \lesssim 4$ keV) to high photon energies ($E \gtrsim 5.5$ keV). We show that this swing can be naturally explained by photon polarization mode conversion at the vacuum resonance in the magnetar atmosphere; the resonance arises from the combined effects of plasma-induced birefringence and QED-induced vacuum birefringence in strong magnetic fields, and the mode conversion is analogous to the MSW effect for neutrino oscillations. This explanation suggests that the atmosphere of 4U 0142 be composed of partially ionized heavy elements (such as Fe), and the surface magnetic field be comparable or less than 10^{14} G, consistent with the dipole field inferred from the measured spindown. It also implies that the spin axis of 4U 0142+61 is aligned with its velocity direction.

neutron stars | x-rays | magnetic fields | polarization

INTRODUCTION

Magnetars are neutron stars (NSs) whose energy outputs (even in quiescence) are dominated by magnetic field dissipations (e.g. Thompson & Duncan 1993; Kaspi & Beloborodov 2017). Recently the NASA/ASI Imaging X-ray Polarimetry Explorer (IXPE) (Weiskopf et al. 2016) reported the detection of linearly polarized x-ray emission from the anomalous x-ray pulsar (AXP) 4U 0142+61, a magnetar with an inferred dipole magnetic field (based the spindown rate) of $\sim 10^{14}$ G (Taverna et al. 2022). This is the first time that polarized x-rays have been detected from any astrophysical point sources. The overall phase-averaged linear polarization degree is $12 \pm 1\%$ throughout the IXPE band (2-8 keV). Interestingly, there is a substantial variation of the polarization signal with energy: the polarization degree is $14 \pm 1\%$ at 2-4 keV and $41 \pm 7\%$ at 5.5-8 keV, while it drops below the detector sensitivity around 4-5 keV, where the polarization angle swings by $\sim 90^\circ$.

To explain the IXPE measurement, particularly the polarization swing, Taverna et al. (2022) suggested that thermal x-rays are emitted from an extended region of the condensed neutron star (NS) surface. In this scenario, the 2-4 keV radiation is dominated by the O-mode (polarized in the plane spanned by the local magnetic field and the photon wave vector), while the 5.5-8 keV radi-

ation by the X-mode (which is orthogonal to the O-mode) because of resonant Compton scattering.

While it is pre-mature to draw any firm conclusion without detailed modeling, the "condensed surface + RCS" scenario may be problematic for several reasons: (i) At the surface temperature of $T_s \simeq 5 \times 10^6$ K and $B_{14} \equiv B/(10^{14} \text{ G}) \simeq 1$, as appropriate for 4U 0142, it is unlikely that the NS surface is in a condensed form, even if the surface composition is Fe (Medin & Lai 2007; Potekhin & Chabrier 2013), simply because the cohesive energy of the Fe solid is not sufficiently large (Medin & Lai 2006). (ii) A stronger surface magnetic field is possible, but the emission from a condensed Fe surface is dominated by the O-mode only for photon energies less than $E_c \simeq 0.1\eta Z^{2/5} B_{14}^{1/5}$ keV, where $\eta \lesssim 1$ (see van Adelsberg et al. 2005; Potekhin et al. 2012). An unrealistically strong field ($B_{14} \gtrsim 10^5$ for $Z = 26$) would be required to make $E_c \gtrsim 4$ keV. (iii) As acknowledged by Taverna et al. (2022), the assumption that the phase-averaged low-energy photons are dominated by the O-mode would imply that the NS spin axis (projected in the sky plane) is orthogonal to the proper motion direction. This is in contradiction to the growing evidence of spin-kick alignment in pulsars. (e.g., Lai et al. 2001; Johnston et al. 2005; Wang et al. 2006; Noutsos et al. 2013; Janka et al. 2022).

In this paper, we show that the 90° linear polarization swing observed in 4U 0142 could be naturally explained by photon mode conversion associated the "vacuum resonance" arising from QED and plasma birefringence in strong magnetic fields. The essential

* E-mail: dong@astro.cornell.edu

physics of this effect was already discussed in Lai & Ho (2003a), where it was shown that for neutron stars with H atmospheres, thermal photons with $E \lesssim 1$ keV are polarized orthogonal to photons with $E \gtrsim 4$ keV, provided that the NS surface magnetic field somewhat less (by a factor of 2) than 10^{14} G. The purpose of this paper is to re-examine the mode conversion effect under more general conditions (particularly the atmosphere composition) and to present new semi-analytic calculations of the polarization signals for parameters relevant to 4U 0142.

VACUUM RESONANCE AND MODE CONVERSION

Quantum electrodynamics (QED) predicts that in a strong magnetic field the vacuum becomes birefringent (e.g., Heisenberg & Euler 1936; Schwinger 1951; Adler 1971; Tsai & Erber 1975; Heyl & Hernquist 1997). Acting by itself, the birefringence from vacuum polarization is significant (with the index of refraction differing from unity by more than 10%) only for $B \gtrsim 300B_Q$, where $B_Q = m_e^2 c^3 / (e \hbar) = 4.414 \times 10^{13}$ G is the critical QED field strength. However, when combined with the birefringence due to the magnetized plasma, vacuum polarization can greatly affect radiative transfer at much smaller field strengths. A “vacuum resonance” arises when the contributions from the plasma and vacuum polarization to the dielectric tensor “compensate” each other (Gnedin et al. 1978; Meszaros & Ventura 1979; Pavlov & Gnedin 1984; Lai & Ho 2002, 2003a,b). Consider x-ray photons propagating in a magnetized plasma that characterizes NS atmospheres. There are two polarization modes: the ordinary mode (O-mode) is mostly polarized parallel to the \mathbf{k} - \mathbf{B} plane, while the extraordinary mode (X-mode) is mostly polarized perpendicular to the \mathbf{k} - \mathbf{B} plane, where \mathbf{k} is the photon wave vector and \mathbf{B} is the external magnetic field (e.g. Meszaros 1992). This description of normal modes applies under typical conditions, except near the vacuum resonance. Throughout the paper, we assume the photon energy E satisfies $u_e = (E_{Be}/E)^2 \gg 1$ and $E_{Bi}/E \ll 1$, where $E_{Be} = \hbar e B / (m_e c) = 1158 B_{14}$ keV and $E_{Bi} = 0.63(Z/A) B_{14}$ keV are the electron and ion cyclotron energies, respectively. In the xyz coordinates with \mathbf{k} along the z -axis and \mathbf{B} in the x - z plane (such that $\hat{\mathbf{B}} \times \hat{\mathbf{k}} = \sin \theta_{kB} \hat{\mathbf{y}}$ (where θ_{kB} is the angle between \mathbf{k} and \mathbf{B}), we write the transverse (xy) electric field of the mode as $\mathbf{E} \propto (iK, 1)$. The mode ellipticity K is given by

$$K_{\pm} = \beta \pm \sqrt{\beta^2 + 1}, \quad (1)$$

where

$$\beta \simeq \frac{u_e^{1/2} \sin^2 \theta_{kB}}{2 \cos \theta_{kB}} \left(1 - \frac{\rho_V}{\rho} \right). \quad (2)$$

For a photon of energy E , the vacuum resonance density is given by

$$\rho_V \simeq 0.964 Y_e^{-1} B_{14}^2 E_1^2 f^{-2} \text{ g cm}^{-3} \quad (3)$$

where $Y_e = \langle Z/A \rangle$ is the electron fraction, $E_1 = E/(1 \text{ keV})$, and $f = f(B)$ is a slowly varying function of B and is of order unity ($f = 1$ for $B \ll B_Q$, $f \simeq 0.991$ at $B_{14} = 1$ and $f \rightarrow (B/5B_Q)^{1/2}$ for $B \gg B_Q$; see Potekhin et al. 2004 for a general fitting formula). For $\rho > \rho_V$ (where the plasma effect dominates the dielectric tensor) and $\rho < \rho_V$ (where vacuum polarization dominates), the photon modes (for typical $\theta_{kB} \neq 0$) are almost linearly polarized; near $\rho = \rho_V$, however, the normal modes become circularly polarized as a result of the “cancellation” of the

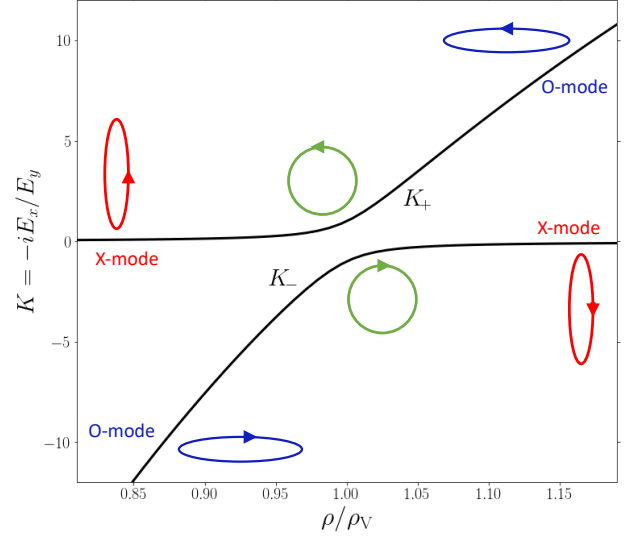


Figure 1. The polarization ellipticity of the photon mode as a function of density near the vacuum resonance. The two curves correspond to the (+) and (-) modes. In this example, the parameters are $B = 10^{14}$ G, $E = 5$ keV, and $\theta_{kB} = 30^\circ$. The ellipticity of a mode is specified by the ratio $K = -iE_x/E_y$, where E_x (E_y) is the photon’s electric field component along (perpendicular to) the \mathbf{k} - \mathbf{B} plane. The O-mode is characterized by $|K| \gg 1$, and the X-mode $|K| \ll 1$.

plasma and vacuum effects (see Fig. 1). The half-width of the vacuum resonance (defined by $|\beta| < 1$) is

$$\epsilon \equiv \frac{\Delta \rho}{\rho_V} = \frac{2 \cos \theta_{kB}}{u_e^{1/2} \sin^2 \theta_{kB}}. \quad (4)$$

When a photon propagates in an inhomogeneous medium, its polarization state will evolve adiabatically (i.e. following the K_+ or K_- curve in Fig. 1) if the density variation is sufficiently gentle. Thus, a X-mode (O-mode) photon will be converted into the O-mode (X-mode) as it traverses the vacuum resonance, with its polarization ellipse rotated by 90° (Fig. 1). This resonant mode conversion is analogous to the Mikheyev-Smirnov-Wolfenstein neutrino oscillation that takes place in the Sun (e.g. Haxton 1995; Bahcall et al. 2003). For this conversion to be effective, the adiabatic condition must be satisfied (Lai & Ho 2002)

$$E \gtrsim E_{\text{ad}} = 2.52 (f \tan \theta_{kB})^{2/3} \left(\frac{1 \text{ cm}}{H_\rho} \right)^{1/3} \text{ keV}, \quad (5)$$

where $H_\rho = |ds/d \ln \rho|$ is the density scale height (evaluated at $\rho = \rho_V$) along the ray. In general, the probability for non-adiabatic “jump” is given by

$$P_J = \exp \left[-\frac{\pi}{2} \left(\frac{E}{E_{\text{ad}}} \right)^3 \right]. \quad (6)$$

The mode conversion probability is $(1 - P_J)$.

CALCULATION OF POLARIZED EMISSION

To quantitatively compute the observed polarized X-ray emission from a magnetic NS, it is necessary to add up emissions from all surface patches of the star, taking account of beaming/anisotropy due to magnetic fields and light bending due to general relativity (e.g. Lai & Ho 2003a; van Adelsberg & Lai 2006; Zane & Turolla 2006; Shabaltas & Lai 2012; Taverna et al. 2020; Caiazzo et

al. 2022). While this is conceptually straightforward, it necessarily involves many uncertainties related to the unknown distributions of surface temperature T_s and magnetic field \mathbf{B} . In addition, the atmosphere composition is unknown, the opacity data for heavy atoms/ions for general magnetic field strengths are not available, and atmosphere models for many surface patches (each with different T_s and \mathbf{B}) are needed. Finally, to determine the phase-resolved lightcurve and polarization, the relative orientations of the line of sight, spin axis and magnetic dipole axis are needed. Given all these complexities, we present a simplified, approximate calculation below. Our goal is to determine under what conditions (in term of the magnetic field strength, surface composition etc) the polarization swing can be produced.

We consider an atmosphere plasma composed of a single ionic species (each with charge Ze and mass Am_p) and electrons. This is of course a simplification, as in reality the atmosphere would consist of multiple ionic species with different ionizations. With the equation of state $P = \rho kT/(\mu m_p)$, hydrostatic balance implies that the column density y at density ρ is given by

$$y = \frac{\rho kT}{\mu m_p g} = 0.41 \frac{\rho_1 T_6}{\mu g_2} \text{ g/cm}^2, \quad (7)$$

where $T = 10^6 T_6$ K is the temperature, $\mu = A/(1+Z)$ is the “molecular” weight, ρ_1 is the density in 1 g/cm^3 , and g_2 is the surface gravity $g = (GM/R^2)(1 - 2GM/Rc^2)^{-1}$ in units of 2×10^{14} (For $M = 1.4M_\odot$, $R = 12 \text{ km}$, we have $g_2 \simeq 1.00$). The density scale-height along a ray is

$$H_\rho \simeq \frac{kT}{\mu m_p g \cos \alpha} = 0.41 \frac{T_6}{\mu g_2 \cos \alpha} \text{ cm}, \quad (8)$$

where α is the angle between the ray and the NS surface normal.

To simplify our calculations, we shall neglect the electron scattering opacity and the bound-bound and bound-free opacities. The former is generally sub-dominant compared to the free-free opacity, while the latter are uncertain or unavailable. The free-free opacity of a photon mode (labeled by i) can be written as

$$\kappa_i = \kappa_0 \xi_i, \quad (9)$$

where the $B = 0$ opacity is (setting the Gaunt factor to unity)

$$\kappa_0 \simeq 9.3 (Z^3/A^2) \rho_1 T_6^{-1/2} E_1^{-3} \mathcal{G}, \quad (10)$$

with $\mathcal{G} = 1 - \exp(-E/kT)$. For the photon mode $\mathbf{E} \propto (iK, 1)$, the dimensionless factor ξ is given by (e.g. Ho & Lai 2001, 2003)

$$\xi = \frac{K^2 \sin^2 \theta_{\text{KB}} + (1 + K^2 \cos^2 \theta_{\text{KB}})/u_e}{1 + K^2}. \quad (11)$$

Figure 2 illustrates the behavior of ξ_X , ξ_O , ξ_+ and ξ_- as a function of density.

For a given photon energy E and wave vector \mathbf{k} (which is inclined by angle α with respect to the surface normal), the transfer equation for mode i (with $i = X, O$ or $i = +, -$) reads

$$\cos \alpha \frac{dI_i}{dy} = \kappa_i \left(I_i - \frac{1}{2} B_\nu \right), \quad (12)$$

where $B_\nu(T)$ is the Planck function and $T = T(y)$ is the temperature profile (to be specified later). To calculate the emergent polarized radiation intensity from the atmosphere, taking account of partial mode conversion, we adopt the following procedure (see van Adelsberg & Lai 2006): (i) We first integrate Eq. (12) for X-mode and O-mode ($i = X, O$) from large y ($= \infty$) to y_V , the column density at which $\rho = \rho_V$. This gives I_{XV} and I_{OV} , the

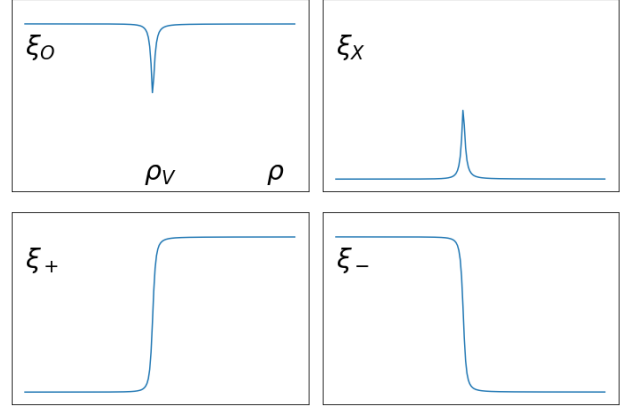


Figure 2. The qualitative behavior of ξ_i (the dimensionless mode opacity; see Eq. 9) as a function of density for photon mode- i (with $i = X, O, +, -$). At the vacuum resonance ($\rho = \rho_V$), ξ_X has a spike, ξ_O has a dip, and ξ_+ and ξ_- have discontinuities. Note that $\xi_+ = \xi_X$ for $\rho < \rho_V$ and $\xi_+ = \xi_O$ for $\rho > \rho_V$, while $\xi_- = \xi_O$ for $\rho < \rho_V$ and $\xi_- = \xi_X$ for $\rho > \rho_V$.

X- and O-mode intensities just before resonance crossing. (ii) We apply partial mode conversion

$$I'_{XV} = I_{XV} P_J + I_{OV} (1 - P_J), \quad (13)$$

$$I'_{OV} = I_{OV} P_J + I_{XV} (1 - P_J), \quad (14)$$

to obtain the mode intensities just after resonance crossing. This partial conversion treatment is valid since the resonance width is small ($\Delta\rho/\rho_V \ll 1$; see Eq. 4). (iii) We then integrate Eq. (12) for X-mode and O-mode again from $y = y_V$ (with the “initial” values I'_{XV} , I'_{OV}) to $y \ll 1$. This then gives the mode intensities emergent from the atmosphere, $I_{X,e}$, $I_{O,e}$.

An alternative procedure is to integrate Eq. (12) for $i = X, O, +, -$ from $y \gg 1$ to $y \ll 1$ (without applying partial mode conversion), which gives the intensities $I_X(0)$, $I_O(0)$, $I_+(0)$ and $I_-(0)$ at $y \simeq 0$. Then apply the partial conversion

$$I_{X,e} = I_X(0) P_J + I_+(0) (1 - P_J), \quad (15)$$

$$I_{O,e} = I_O(0) P_J + I_-(0) (1 - P_J), \quad (16)$$

where P_J is evaluated at $y = y_V$.

It is straightforward to show that the above two procedures are equivalent. For example, after obtaining I'_{XV} , we can get the emergent X-mode intensity by

$$I_{X,e} = I'_{XV} \exp\left(-\frac{\tau_{XV}}{\cos \alpha}\right) + \Delta I_{XV}, \quad (17)$$

where $\tau_{XV} = \int_0^{y_V} \kappa_X dy$ is the optical depth of X-mode (measured along the surface normal) at $y = y_V$, and ΔI_{XV} is the contribution to $I_{X,e}$ from the region $0 < y < y_V$:

$$\Delta I_{XV} = \int_0^{\tau_{XV}/\cos \alpha} \exp\left(-\frac{\tau_X}{\cos \alpha}\right) \frac{1}{2} B_\nu(T) \frac{d\tau_X}{\cos \alpha}. \quad (18)$$

On the other hand, when integrating Eq. (12) for $i = X$ from $y \gg 1$ to $y \ll 1$, we obtain

$$I_X(0) = I_{XV} \exp\left(-\frac{\tau_{XV}}{\cos \alpha}\right) + \Delta I_{XV}. \quad (19)$$

Similarly,

$$I_+(0) = I_{OV} \exp\left(-\frac{\tau_{XV}}{\cos \alpha}\right) + \Delta I_{XV}. \quad (20)$$

It is easy to see that Eq. (17) together with Eq. (13) (the first procedure) and Eq. (15) with Eqs. (19)-(20) (the second procedure) yield the same emergent $I_{X,e}$.

Decoupling densities and Critical Field

Before presenting our sample results, it is useful to estimate photon decoupling densities for different modes and the condition for polarization swing.

When the vacuum polarization effect is neglected ($\rho_V = 0$), $|\beta| \gg 1$ at all densities (for typical θ_{kB} 's not too close to 0), the ξ -factors for the O-mode ($|K| \gg 1$) and for the X-mode (with $|K| \ll 1$) are

$$\xi_O \simeq \sin^2 \theta_{kB}, \quad \xi_X \simeq \frac{1}{u_e \sin^2 \theta_{kB}}. \quad (21)$$

The decoupling locations of the O-mode and X-mode photons are determined by the condition

$$\int_0^{y_{O,X}} \kappa_{O,X} \frac{dy}{\cos \alpha} = 2/3. \quad (22)$$

The corresponding decoupling densities can be estimated as

$$\rho_O = \xi_O^{-1/2} \rho_0, \quad (23)$$

$$\rho_X = \xi_X^{-1/2} \rho_0, \quad (24)$$

where the “zero-field” decoupling density is

$$\rho_0 \simeq 0.59 \left(\frac{\mu g_2 \cos \alpha}{\mathcal{G}} \right)^{1/2} \left(\frac{E_1}{Z} \right)^{3/2} \left(\frac{A}{T_6^{1/4}} \right) \text{ g cm}^{-3}. \quad (25)$$

The effect of the vacuum resonance on the radiative transfer depends qualitatively on the ratios ρ_V/ρ_O and ρ_V/ρ_X , given by

$$\frac{\rho_V}{\rho_O} = \left(\frac{B}{B_{OV}} \right)^2, \quad \frac{\rho_V}{\rho_X} = \frac{B}{B_{XV}}, \quad (26)$$

where

$$B_{OV} = 7.8 \times 10^{13} \left(\frac{\mu g_2 \cos \alpha}{Z \mathcal{G} E_1 \sin^2 \theta_{kB}} \right)^{1/4} \left(\frac{f}{T_6^{1/8}} \right) \text{ G}, \quad (27)$$

$$B_{XV} = 7.1 \times 10^{16} \left(\frac{\mu g_2 \cos \alpha}{Z \mathcal{G} E_1^3} \right)^{1/2} \left(\frac{f^2 \sin \theta_{kB}}{T_6^{1/4}} \right) \text{ G}. \quad (28)$$

Clearly, the condition $B \ll B_{XV}$ or $\rho_V \ll \rho_X$ is satisfied for almost all relevant NS parameters of interest, while B_{OV} defines the critical field strength for the 90° polarization swing (see Figs. 3-4): If $B \lesssim B_{OV}$, the emergent radiation is dominated by the X-mode for $E \lesssim E_{ad}$ and by the O-mode for $E \gtrsim E_{ad}$; if $B \gtrsim B_{OV}$, the X-mode is dominant for all E 's.

We can quantify the role of B_{OV} more precisely by estimating how vacuum resonance affects the photon decoupling densities. In the limit of no mode conversion (i.e. $E \ll E_{ad}$), it is appropriate to consider the transport of X-mode and O-mode, with the mode opacities modified around the vacuum resonance (see Fig. 2). The O-mode opacity has a dip near $\rho = \rho_V$ (where $\xi \simeq \sin^2 \theta_{kB}/2$), and since the resonance width $\Delta\rho/\rho_V \ll 1$, the decoupling density $\rho_{O'}$ is almost unchanged from the no-vacuum value, i.e. $\rho_{O'} \simeq \rho_O$. On the other hand, the X-mode opacity has a large spike at $\rho = \rho_V$ (where $\xi = \sin^2 \theta_{kB}/2$) compared to the off-resonance value ($\xi \sim u_e^{-1}$). The X-mode optical depth across the resonance (from $\rho_V - \Delta\rho$ to $\rho_V + \Delta\rho$) is of order $\Delta\tau_V \sim \epsilon(\rho_V/\rho_O)^2$, where ϵ is

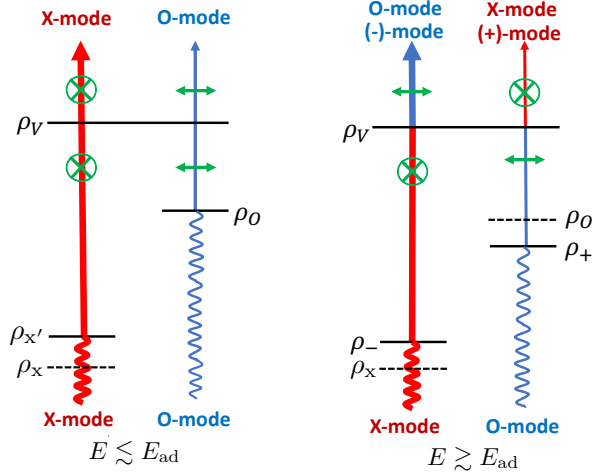


Figure 3. A schematic diagram illustrating how vacuum resonance affects the polarization state of the emergent radiation from a magnetized NS atmosphere. This diagram applies to the $B \lesssim B_{OV}$ regime so that the vacuum resonance density ρ_V is less than the O-mode decoupling density ρ_O . For $E \lesssim E_{ad}$, the photon evolves nonadiabatically across the vacuum resonance (for θ_{kB} not too close to 0), thus the emergent radiation is dominated by the X-mode. For $E \gtrsim E_{ad}$, the photon evolves adiabatically, with its plane of polarization rotating by 90° across the vacuum resonance, and thus the emergent radiation is dominated by the O-mode. The plane of linear polarization at low energies is therefore perpendicular to that at high energies.

given by Eq. (4). Thus the modified X-mode decoupling density is $\rho_{X'} \simeq \rho_V$ for $\Delta\tau_V \gtrsim 1$ and

$$\rho_{X'} \sim \rho_X \left[1 - \epsilon (\rho_V/\rho_O)^2 \right]^{1/2} \quad (29)$$

for $\Delta\tau_V \lesssim 1$.

In the limit of complete mode conversion (i.e. $E \gg E_{ad}$), it is appropriate to consider the transport of (+)-mode and (-)-mode, with the mode opacities exhibiting a discontinuity at $\rho = \rho_V$ (see Fig. 2). The (+)-mode decoupling density ρ_+ is given by

$$\rho_+^2 \simeq \rho_O^2 + \left(1 + \frac{\xi_X}{\xi_O} \right) \rho_V^2 \simeq \rho_O^2 + \rho_V^2. \quad (30)$$

The (-)-mode decoupling density ρ_- is only affected by the vacuum resonance if $\rho_O > \rho_V$. Thus

$$\rho_- = \rho_O \quad \text{for } \rho_O < \rho_V \quad (31)$$

and

$$\rho_-^2 = \rho_V^2 + \frac{\xi_O}{\xi_X} (\rho_O^2 - \rho_V^2) \quad \text{for } \rho_O > \rho_V \quad (32)$$

For general E 's with partial mode conversion, the emergent mode intensities are approximately given by

$$I_{O,e} \simeq \frac{1}{2} P_J B_\nu(\rho_O) + \frac{1}{2} (1 - P_J) B_\nu(\rho_-), \quad (33)$$

$$I_{X,e} \simeq \frac{1}{2} P_J B_\nu(\rho_{X'}) + \frac{1}{2} (1 - P_J) B_\nu(\rho_+), \quad (34)$$

where (for example) $B_\nu(\rho_O)$ is the Planck function evaluated at $\rho = \rho_O$. These results are schematically depicted in Figs. 3-4.

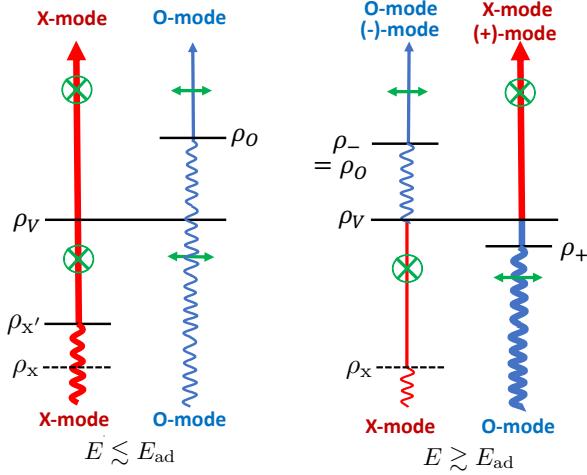


Figure 4. Same as Fig. 3, except for the $B \gtrsim B_{OV}$ regime ($\rho_V > \rho_O$), in which the emergent radiation is always dominated by X-mode for all E 's.

Results

To compute the polarized radiation spectrum emergent from a NS atmosphere patch using the method presented above (Eq. 12 with Eqs. 13-14 or with Eqs. 15-16), we need to know the atmosphere temperature profile $T(y)$. This can only be obtained by self-consistent atmosphere modeling, which has only been done for a small number of cases (in terms of the local T_s , B and composition). Here, to explore the effect of different B and compositions, we consider two approximate models:

- Model (i): We use the profile $T_H(y)$ for the $T_s = 5 \times 10^6$ K H atmosphere model with a vertical field $B = 10^{14}$ G (van Adelsberg & Lai 2006; this model correctly treats the partial mode conversion effect), and re-scale it to take account of the modification of the free-free opacity for different Z , A (so that the re-scaled profile yields the same effective surface temperature T_s):

$$T(y) = (2\mu Z^3/A^2)^{1/8.5} T_H(y). \quad (35)$$

- Model (ii): We use a smooth (monotonic) fit to the T_H profile, given by

$$\log_{10} T_H(y) = 0.11 + 0.147 [\log_{10}(0.4y) + 3], \quad (36)$$

and then apply Eq. (35) for re-scaling.

Figures 5-6 show a sample of our results for the polarization degree of the emergent radiation, defined by

$$P_L \equiv \frac{I_{X,e} - I_{O,e}}{I_{X,e} + I_{O,e}}. \quad (37)$$

We see that for the H and He atmospheres (Fig. 5), P_L transitions from being positive at low E 's to negative at high E 's for $B_{14} \lesssim 0.5$, in agreement with the critical field estimate (Eq. 27). The transition energy (where $P_L = 0$) is approximately given by E_{ad} , and has the scaling $E_{ad} \propto (\mu \tan^2 \theta_B)^{1/3}$, where θ_B is the angle between the surface B and the surface normal (see Eq. 5). To obtain a transition energy of 4 – 5 keV (as observed for 4U 0142) would require most of the emission comes from the surface region with $\theta_B \gtrsim 70^\circ$.

On the other hand, for a partially ionized heavy-element atmosphere (such that μ/Z is much larger than unity), the critical field B_{OV} can be increased (see Eq. 27). Figure 6 shows that at

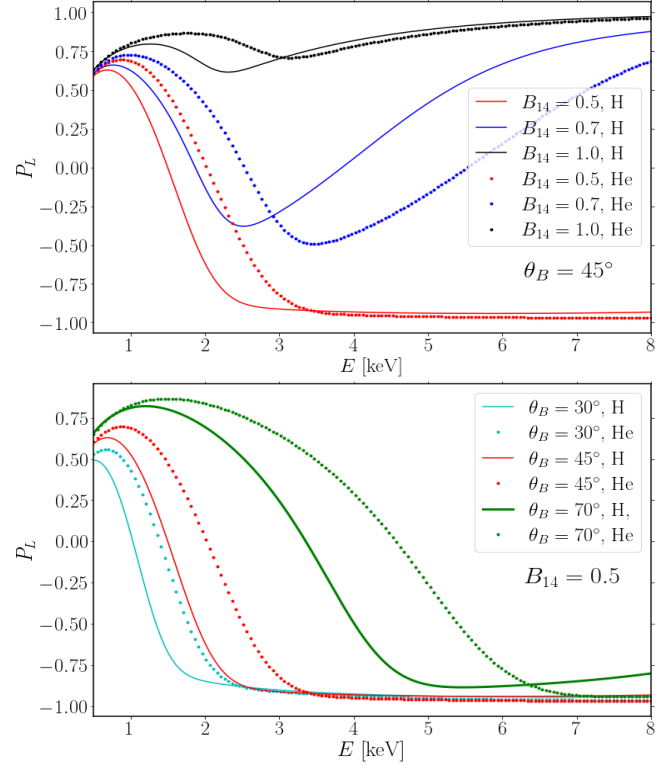


Figure 5. Polarization degree P_L (defined by Eq. 37) of the emergent radiation normal to the surface as a function of the photon energy E for H and He atmospheres with different magnetic field strengths and directions (θ_B , the angle between the surface B and the surface normal vector). All results are based on the temperature profile Model (ii).

$B_{14} = 1$, a $Z = 2$, $A = 56$ atmosphere can have a sign change in P_L around $E \sim 3 - 5$ keV (depending on the θ_B value).

To determine the observed polarization signal, we must consider the propagation of polarized radiation in the NS magnetosphere, whose dielectric property in the X-ray band is dominated by vacuum polarization (Heyl et al. 2003). As a photon propagates from the NS surface through the magnetosphere, its polarization state evolves following the varying magnetic field it experiences, up to the “polarization-limiting radius” r_{pl} , beyond which the polarization state is frozen. It is convenient to set up a fixed coordinate system XYZ , where the Z -axis is along the line-of-sight and the X -axis lies in the plane spanned by the Z -axis and Ω (the NS spin angular velocity vector). The polarization-limiting radius r_{pl} is determined by the condition $\Delta k = 2|d\phi_B/ds|$, where $\Delta k = |k_X - k_O|$ is the difference in the wavenumbers of the two photon modes, and $\phi_B(s)$ is the azimuthal angle of the magnetic field along the ray (s measures the distance along the ray). For a NS with surface dipole field B_d and spin frequency $\nu = \Omega/(2\pi)$, we have (van Adelsberg & Lai 2006) $r_{pl}/R \sim 150 (E_1 B_{d,14}^2/\nu_1)^{1/6}$, where $B_{d,14} = B_d/(10^{14} \text{ G})$ and $\nu_1 = \nu/\text{Hz}$. Note that since $R \ll r_{pl} \ll r_l$ [with $r_l = c/\Omega$ the light-cylinder radius], only the dipole field determines r_{pl} . Regardless of the surface magnetic field structure, the radiation emerging from most atmosphere patches with mode intensities $I_{X,e}$ and $I_{O,e}$ evolves adiabatically in the magnetosphere such that the radiation at $r > r_{pl}$ consists of approximately the same $I_{X,e}$ and $I_{O,e}$, with a small mixture of circular polarization generated around r_{pl} (van Adelsberg & Lai 2006). The exception occurs for those rays that encounter the quasi-

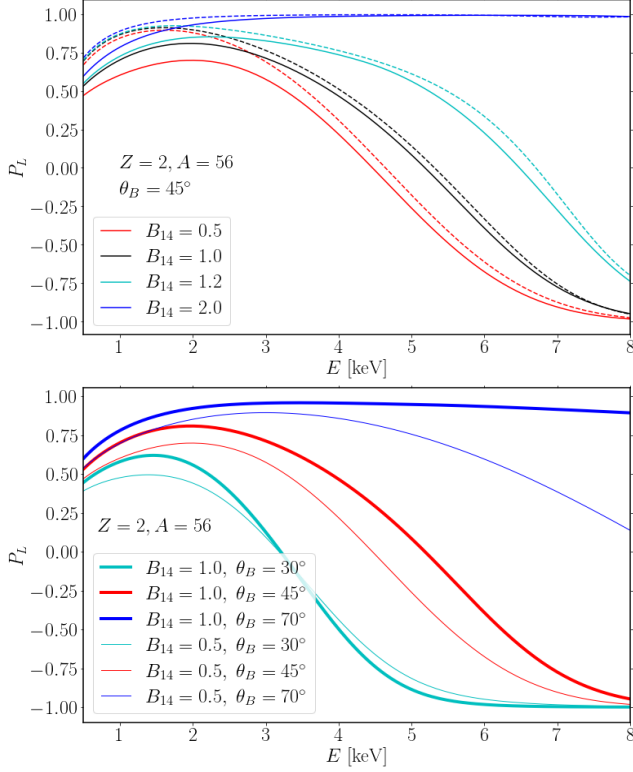


Figure 6. Similar to Fig. 5, except for partially ionized Fe atmospheres with $Z = 2$, $A = 56$. In the upper panel, the solid/dashed lines are for Model (i)/(ii). In the lower panel, the results are shown for Model (i).

tangential point (where the photon momentum is nearly aligned with the local magnetic field) during their travel from the surface to r_{pl} (Wang & Lai 2009). Since only a small fraction of the NS surface radiation is affected by the quasi-tangential propagation, we can neglect its effect if the observed radiation comes from a large area of the NS surface. Let the azimuthal angle of the \mathbf{B} field at r_{pl} be $\phi_B(r_{\text{pl}})$ in the the XYZ coordinate system. The observed Stokes parameters (normalized to the total intensity I) are then given by

$$Q/I = -P_L \cos 2\phi_B(r_{\text{pl}}), \quad (38)$$

$$U/I = -P_L \sin 2\phi_B(r_{\text{pl}}). \quad (39)$$

Note that when $r_{\text{pl}} \ll r_l$, the transverse (XY) component of $\mathbf{B}(r_{\text{pl}})$ is opposite to the transverse component of the magnetic dipole moment $\boldsymbol{\mu}$, thus $\phi_B(r_{\text{pl}}) \simeq \pi + \phi_\mu$, where ϕ_μ is the azimuthal angle of $\boldsymbol{\mu}$.

For determine the emission from the whole NS surface, we need to add up contributions from different patches (area element dS), including the effect of general relativity (Pechenick et al. 1983; Beloborodov 2002). For example, the observed spectral fluxes F_I , F_Q (associated with the intensities I , Q) are

$$F_I = g_r^3 \int \frac{dS \cos \alpha}{D^2} (I_{X,e} + I_{O,e}), \quad (40)$$

$$F_Q = g_r^3 \int \frac{dS \cos \alpha}{D^2} (I_{O,e} - I_{X,e}) \cos 2\phi_B(r_{\text{pl}}), \quad (41)$$

where $g_r \equiv (1 - 2GM/Rc^2)^{1/2}$ and α is the angle between the ray and the surface normal at the emission point). Clearly, to compute F_I , F_Q and F_U requires the knowledge of the distributions of NS surface temperature and magnetic field, as well as various angles (the relative orientations between the line of sight, the spin

axis and the dipole axis). This is beyond the scope of the paper. Nevertheless, our results depicted in Figs. 5-6 (with different values of local field strengths and orientations) show that the 90° linear polarization swing observed in AXP 4U 0142 can be explained by emission from a partially ionized heavy-element atmosphere with surface field strength about 10^{14} G, or a H/He atmosphere with $B_{14} \lesssim 0.5$ and a more restricted surface field geometry (i.e. most of the radiation comes from the regions with $\theta_B \gtrsim 70^\circ$).

DISCUSSION

We have shown that the observed the x-ray polarization signal from AXP 4U 0142, particularly the 90° swing around 4-5 keV, can be naturally explained by the mode conversion effect associated vacuum resonance in the NS atmosphere. In this scenario, the 2-4 keV emission is dominated by the X-mode, while the 5-8 keV emission by the O-mode as a result of the adiabatic mode conversion from the X-mode to the O-mode. This would resolve some of the difficulties associated with the alternative interpretations of the X-ray polarization data regarding the physical state of the NS surface and the spin-kick correlation (see Section 1).

It is important to note that in our scenario, the existence of the X-ray polarization swing depends sensitively on the actual value of the magnetic field on the NS surface (see Eq. 27). To explain the observation of AXP 4U 0142, the magnetic fields in most region of the NS surface must be less than about 10^{14} G, and a lower field strength would be preferred in terms of producing the polarization swing robustly (for a wide range of geometrical parameters). Using the pulsar spindown power derived from force-free electrodynamics simulations (Spitkovsky 2006), $L_{\text{sd}} = (\mu^2 \Omega^4 / c^3)(1 + \sin^2 \theta_{s\mu})$ (where $\theta_{s\mu}$ is the angle between the magnetic dipole $\boldsymbol{\mu}$ and the spin axis), we find that for the observed P , \dot{P} of 4U 0142, the dipole field at the magnetic equator is $B_d = 1.1 \times 10^{14} I_{45}^{1/2} R_6^{-3} (1 + \sin^2 \theta_{s\mu})^{-1/2}$ G, where R_6 is the NS radius in units of 10^6 cm, and I_{45} is the moment of inertia in units of 10^{45} g cm². Note that with $R_6 \simeq 1.3$ (see Miller et al. 2021; Raaijmakers et al. 2021), the above estimate is reduced by a factor of 2. In addition, if the magnetar possesses a relativistic wind with luminosity $L_w \gtrsim L_{\text{sd}}$, the wind can open up field lines at $r_{\text{open}} \sim (B_d^2 R^6 c / L_w)^{1/4} \lesssim c/\Omega$ and significantly enhance the spindown torque (Thompson & Blaes 1998; Harding et al. 1999; Thompson et al. 2000). This would imply that a smaller B_d is needed to produce the observed \dot{P} in 4U 0142. Thus, the observation of X-ray polarization swing is consistent with the indirectly “measured” dipole field, and requires that the high-order multipole field components be not much stronger than the dipole field.

Finally, we reiterate some of the caveats of our work: we have not attempted to calculate the synthetic polarized radiation from the whole NS and to compare with the X-ray data from AXP 4U 0142 in detail; our treatment of partially ionized heavy-element magnetic NS atmospheres is also approximate in several aspects (e.g., bound-free opacities are neglected, the vertical temperature profiles are assumed based on limited H atmosphere models). At present, these caveats are unavoidable, given the uncertainties (and large parameter space needed to do a proper survey) in the surface temperature and magnetic field distributions on the NS, and the fact that self-consistent heavy-element atmospheres models for general magnetic field strengths and orientations have not been constructed, especially in the regime where the vacuum resonance effects are important. Nevertheless, our results clearly demonstrate the important role played by the vacuum resonance in producing

the observed X-ray polarization signature from magnetars. The observation of AXP 4U 0142 by IXPE has now opened up a new window in studying the surface environment of NSs. Future X-ray polarization mission (such as eXTP; see Zhang et al. 2019) will provide more detailed observational data. Comprehensive theoretical modelings of magnetic NS atmosphere and surface radiation will be needed to confront these observations.

REFERENCES

- Adler, S.L. 1971, *Ann. Phys.*, 67, 599
- Bahcall, J.N., Gonzalez-Garcia, M.C., & Pena-Garay, C. 2003, *J. High Energy Phys. JHEP02*, 009
- Beloborodov, A.M. 2002, *ApJ*, 566, L85
- Caiazzo, I., Gonzalez-Caniulef, D., Heyl, J., Fernandez, R. 2022, *MNRAS*, 514, 5024
- Gnedin, Yu.N., Pavlov, G.G., & Shibano, Yu.A. 1978, *Sov. Astron. Lett.*, 4(3), 117
- Harding A. K., Contopoulos I., Kazanas D., 1999, *ApJ*, 525, L125
- Haxton, W.C. 1995, *Ann. Rev. Astron. Astrophys.*, 33, 459
- Heisenberg, W. & Euler, H. 1936, *Z. Physik*, 98, 714
- Heyl, J.S. & Hernquist, L. 1997, *J. Phys. A* 30, 6485
- Heyl, J.S., Shaviv, N.J., & Lloyd, D. 2003, *MNRAS*, 342, 134
- Ho, W.C.G., & Lai, D. 2003, *MNRAS*, 338, 233
- Janka, H.-T., Wongwathanarat, A., Kramer, M. 2022, *ApJ*, 926, 9
- Johnston, S., et al. 2005, *MNRAS*, 364, 1394
- Kaspi V. M., Beloborodov A. M., 2017, *ARA&A*, 55, 261
- Lai, D., Chernoff, D.F., Cordes, J.M. 2001, *ApJ*, 549, 1118
- Lai, D. & Ho, W.C.G. 2002, *ApJ*, 566, 373
- Lai, D., Ho, W.C.G. 2003a, *PRL*, 91, 071101
- Lai, D., Ho, W.C.G. 2003b, *ApJ*, 588, 962
- Medin, Z., Lai, D. 2006, *Phys. Rev. A* 74, 062508
- Medin, Z., Lai, D. 2007, *MNRAS*, 382, 1833
- Mészáros, P. 1992, *High-Energy Radiation from Magnetized Neutron Stars* (Univ. Chicago Press, Chicago)
- Mészáros, P. & Ventura, J. 1979, *Phys. Rev. D* 19, 3565
- Miller, M.C. et al. 2021, *ApJ*, 918, L28
- Noutsos, A., et al. 2013, *MNRAS*, 430, 2281
- Pavlov, G.G. & Gnedin, Yu.N. 1984, *Sov. Sci. Rev. E: Astrophys. Space Phys.* 3, 197
- Pechenick, K.R., Ftaclas, C., & Cohen, J.M. 1983, *ApJ*, 274, 846
- Potekhin, A., et al. 2004, *ApJ*, 612, 1034
- Potekhin, A., Chabrier, G. 2013, *A&A*, 550, A43
- Potekhin, A.Y., Suleimanov, V.F., van Adelsberg, M., Werner, K. 2012, *A&A*, 546, A121
- Raaijmakers, G. et al. 2021, *ApJ*, 918, L29
- Schwinger, J. 1951, *Phys. Rev.*, 82, 664
- Shabaltas, N., Lai, D. 2012, *ApJ*, 748, 148
- Spitkovsky, A. 2006, *ApJ*, 648, L51
- Taverna, R., Turolla, R., Suleimanov, V., Potekhin, A.Y., Zane, S. 2020, *MNRAS*, 492, 5057
- Taverna, R. et al. 2022, *Science*, submitted (arXiv:2205.08898)
- Tsai, W.Y., Erber, T. 1975, *Phys. Rev. D*, 12, 1132
- Thompson C., Blaes O., 1998, *Phys. Rev. D* 57, 3219
- Thompson, C., Duncan R. C. 1993, *ApJ*, 408, 194
- Thompson C., Duncan R. C., Woods P. M., Kouveliotou C., Finger M. H., van Paradijs J., 2000, *ApJ*, 543, 340
- van Adelsberg, M., Lai, D., Potekhin, A.Y., Arras, P. 2005, *ApJ*, 628, 902
- van Adelsberg, M., Lai, D. 2006, *MNRAS*, 373, 1495
- Wang, C., Lai, D., Han, J.L. 2006, *ApJ*, 639, 1007
- Weisskopf, M.C. et al. 2016, *Proc. SPIE* 9905, 990517; <https://doi.org/10.1117/12.2235240>
- Zane, S., & Turolla, R. 2006, *MNRAS*, 366, 727
- Zhang, Shuangnan, et al. 2019, *Science China Physics, Mechanics & Astronomy*, 62, 29502